J. Fluid Mech. (1997), *vol.* 338, *pp.* 127–155

Experimental assessment of fractal scale similarity in turbulent flows. Part 3. Multifractal scaling

By RICHARD D. FREDERIKSEN,[1] WERNER J. A. DAHM[1] AND DAVID R. DOWLING[2]

[1] Department of Aerospace Engineering, The University of Michigan Ann Arbor, MI 48109-2118, USA

[2] Department of Mechanical Engineering and Applied Mechanics, The University of Michigan Ann Arbor, MI 48109-2125, USA

(Received 22 May 1996 and in revised form 11 September 1996)

Earlier experimental assessments of fractal scale similarity in geometric properties of turbulent flows are extended to assess the applicability of multifractal scale-similarity in the conserved scalar field $\zeta(\boldsymbol{x}, t)$ and in the true scalar energy dissipation rate field $\boldsymbol{\nabla}\zeta \cdot \boldsymbol{\nabla}\zeta(\boldsymbol{x}, t)$. Fully resolved four-dimensional spatio-temporal measurements from a turbulent flow at $Re_\lambda \approx 41$ and $Re_\delta \approx 3000$ are analysed. The utility of various classical constructs for identifying multifractal scale similarity in data records of finite length is examined. An objective statistical criterion based on the maximum allowable scale-to-scale variation $L_1(\epsilon)$ in multiplier distributions $\langle P(M_\epsilon)\rangle$ obtained from multifractal gauge fields is developed to allow accurate discrimination between multifractal and non-multifractal scaling in finite-length experimental data records. Results from analyses of temporal intersections show that for scales greater than $0.03\,\lambda_\nu/u$, corresponding to $1.4\,\lambda_D/u$, the scalar dissipation field clearly demonstrates a scale-invariant similarity consistent with a multiplicative cascade process that can be modelled with a bilinear multiplier distribution. However, the conserved scalar field from precisely the same data does not follow any scale similarity consistent with a multiplicative cascade at scales below $0.5\,\lambda_\nu/u$. At larger scales, there are indications of a possible scale-invariant similarity in the scalar field, but with a fundamentally different multiplier distribution.

1. Introduction

The highly intermittent nature of gradient quantities associated with velocity and scalar fields in turbulent flows is the principal hindrance in the formulation of accurate statistical closure methods for modelling these fields. In developing such models, one of the key objectives is identification of the proper scale similarity rules that govern scalar and velocity gradients over lengthscales and timescales that are sufficiently small for the natural equilibrium among scales to be established. In two previous papers (Frederiksen, Dahm & Dowling 1996, 1997; hereinafter referred to as Parts 1 and 2) we used experimental data to assess the applicability of concepts from fractal geometry for characterizing scale similarity in one-, two-, and three-dimensional spatial and temporal intersections with various geometric properties of turbulent flows. Those studies introduced objective statistical methods for determining if a given data record with finite length was 'as fractal as a known fractal gauge set having the same record length'. Criteria were established for comparisons with both deterministically and stochastically self-similar fractal gauge sets. The main result was that the geometry of

scalar isosurfaces was found to be inconsistent with the concept of uniform fractal scale similarity. However, the scalar energy dissipation support geometry from precisely the same data showed uniform fractal scale similarity over the entire range of scales. In the present study, these experimental assessments are extended to examine the applicability of multifractal concepts for characterizing scale similarity in the entire conserved scalar field $\zeta(\boldsymbol{x}, t)$ and scalar energy dissipation rate field $\boldsymbol{\nabla}\zeta \cdot \boldsymbol{\nabla}\zeta(\boldsymbol{x}, t)$ in turbulent flows.

Fractal scaling assessments such as those in Parts 1 and 2 are concerned solely with characterizing the geometry of a subset of the four-dimensional space $(\boldsymbol{x}, t)$ on which some property associated with a field $\mu(\boldsymbol{x}, t)$ is found. For the scalar dissipation field, for instance, the set considered was the dissipation support, namely the subset of $(\boldsymbol{x}, t)$ where the dissipation $\boldsymbol{\nabla}\zeta \cdot \boldsymbol{\nabla}\zeta(\boldsymbol{x}, t)$ exceeded a chosen threshold value, and it was the geometric scale similarity properties of this set itself that were of interest. If a particular type of scale similarity was applicable, then the set was termed 'fractal' and its geometric scale similarity properties were characterized by its fractal dimension.

Multifractal scaling, on the other hand, is not concerned simply with the geometry of any one particular subset, but rather with all the geometries of a specific family of subsets that, collectively, describe the entire field $\mu(\boldsymbol{x}, t)$. For intermittent but continuous fields, the subsets can be parameterized by local power law exponents in $\mu(\boldsymbol{x}, t)$, or equivalently by local exponents α in a set of measures $\mu_\epsilon(\boldsymbol{x}, t)$ derived from $\mu(\boldsymbol{x}, t)$, which for certain α describe local singularities in $\mu(\boldsymbol{x}, t)$. If the geometries of all the subsets associated with all the α display fractal scale similarity, then the field is termed 'multifractal'. In that case, it is the fractal dimension f of the subset associated with each α that is of interest, and the resulting $f(\alpha)$ then characterizes the complete scale-similarity properties of the entire field $\mu(\boldsymbol{x}, t)$.

Early work (Mandelbrot 1974) used what were effectively primitive multifractal concepts to predict divergence of higher-order moments of the turbulent energy dissipation. Subsequent developments along similar lines led to the β-model of Frisch, Sulem & Nelkin (1978) and the random β-model of Benzi *et al.* (1984) for the distribution of energy dissipation in turbulent flows. The modern mathematical basis of multifractal theory was subsequently developed by Hentschel & Procaccia (1983), Frisch & Parisi (1985), and Halsey *et al.* (1986). Since then, there has been extensive activity aimed at applying this formalism to characterize various aspects of turbulent flows. Sreenivasan (1991*a*, *b*) reviews much of the application of multifractal theory in the context of turbulent flows, and models based on these multifractal concepts have begun to appear.

However, direct experimental assessments of the applicability of multifractal scaling to the similarity properties of turbulent flows have been limited. An early investigation by Meneveau & Sreenivasan (1987), and a more detailed study by Meneveau & Sreenivasan (1991), concluded that the turbulent energy dissipation field exhibited multifractal characteristics. Meneveau (1991) subsequently used wavelet analyses to investigate scale similarity in the dissipation field, and found results consistent with multifractal scaling. More recently, Sreenivasan & Stolovitzky (1995) examined scale similarity in detail and suggested the possibility of correlations in the 'cascade' process. These assessments, however, were all based on the surrogate quantity $(\partial u/\partial t)^2$ in place of the true kinetic energy dissipation rate field $2\nu \boldsymbol{\Sigma} : \boldsymbol{\Sigma}(\boldsymbol{x}, t)$, owing to the difficulty in measuring directly the full strain rate tensor field $\boldsymbol{\Sigma}(\boldsymbol{x}, t)$ in turbulent flows (Tsinober, Kit & Dracos 1992; Su & Dahm 1996*a*, *b*). In contrast, the true scalar energy dissipation rate field $D\,\boldsymbol{\nabla}\zeta \cdot \boldsymbol{\nabla}\zeta(\boldsymbol{x}, t)$ in turbulent flows has in recent years become accessible via direct measurements of the full scalar gradient vector field $\nabla\zeta(\boldsymbol{x}, t)$ (e.g.

Dahm, Southerland & Buch 1991; Southerland & Dahm 1994, 1996). Such dynamically passive conserved scalar fields carry the signature of dynamics in the velocity field in turbulent flows, and thus provide indirect access to the scale similarity properties of the underlying flow itself.

Prediction and early measurements of a multifractal scalar energy dissipation field in turbulent flows were reported by Prasad, Meneveau & Sreenivasan (1988) and Sreenivasan & Prasad (1989). Numerical and analytical work by Ott & Antonsen (1989) and Varósi, Antonsen & Ott (1991) indicate multifractal scalar dissipation fields to be a signature of chaotic flows (suggesting a possible link between mixing by turbulent motion and by chaotic advection). Possible multifractal similarity in the conserved scalar field in turbulent flows has been postulated by Chechetkin, Lutovinov & Turygin (1990) and Shivamoggi (1992), with no experimental evidence having yet been presented.

The present study uses experimental data from fully resolved four-dimensional spatio-temporal measurements of the conserved scalar field $\zeta(\boldsymbol{x}, t)$ and scalar energy dissipation rate field $\boldsymbol{\nabla}\zeta \cdot \boldsymbol{\nabla}\zeta(\boldsymbol{x}, t)$ in turbulent flows to examine the applicability of multifractal concepts for characterizing the scale-similarity properties of these fields. We develop strict objective statistical criteria based on known multifractal gauge fields to discriminate between multifractal and non-multifractal data, and then apply these to test the hypothesis of multifractal scale similarity in the fields examined. In §2 below we briefly summarize the experimental data used in the present study, and in §3 we review the essential concepts of multifractal theory relevant to the present study. Following this, §4 evaluates the utility of various constructs for identifying multifractal scale similarity in data records of finite length, and then develops strict criteria for judging the applicability of multifractal scaling in the present data. Results from evaluation of these criteria for the $\zeta(\boldsymbol{x}, t)$ and $\boldsymbol{\nabla}\zeta \cdot \boldsymbol{\nabla}\zeta(\boldsymbol{x}, t)$ fields are given in §5, and conclusions regarding the applicability of multifractal scaling concepts for characterizing the scale-similarity properties of turbulent flows are then drawn in §6.

2. Data characteristics

The fully resolved four-dimensional spatio-temporal experimental data used in this study are the same as those used in Parts 1 and 2, and have been described in detail in Part 1. Briefly, these data were obtained using laser-induced fluorescence for the mixing of a dynamically passive $Sc \approx 2000$ dye in the self-similar far field of an axisymmetric turbulent jet in water. The measurement technique is described in detail in Dahm *et al.* (1991) and Southerland & Dahm (1994, 1996). The concentration field $\zeta(\boldsymbol{x}, t)$ of a laser fluorescent dye carried by the jet fluid was measured repeatedly in time at as many as 256^3 points within a small three-dimensional spatial volume in the jet far field. A highly collimated laser beam was swept in a raster fashion through this volume, and the resulting laser induced fluorescence from dye-containing fluid imaged onto a high-speed 256×256 element photodiode array. The array output was serially acquired at 8-bits true digital depth and continuously written in real time at rates up to 9.1 MB s^{-1} to a 3.1 GB high-speed parallel-transfer disk bank capable of accommodating more than 50000 such 256^2 data planes. The resulting measured fluorescence intensity field was subsequently converted to the true dye concentration as described in Southerland & Dahm (1994, 1996).

As detailed in Parts 1 and 2 (see also Southerland & Dahm 1994, 1996), the spatial and temporal resolution achieved resolves all the fine-scale structure associated with the local turbulent mixing process in the flow. The characteristic scale of the pixel image

volume $(\Delta x \Delta y \Delta z)^{1/3}$ and its maximum dimension (Δz) are less than half the local strain-limited molecular diffusion lengthscale λ_D, and thus less than $\frac{1}{20}$ of the local Kolmogorov scale $\lambda_K \equiv (\nu^3/\epsilon)^{1/4}$. Similarly, the intervolume time in all cases was less than half the scalar diffusion scale advection time $T_v \equiv \lambda_D/u$, and thus less than $\frac{1}{200}$ the Kolmogorov timescale $\tau_K \equiv (\nu/\epsilon)^{1/2}$. Together with the high signal quality achieved, the resulting spatio-temporal resolution allows accurate simultaneous differentiation of the measured conserved scalar field data $\zeta(\boldsymbol{x}, t)$ in all three spatial dimensions and in time to determine all three components of the true scalar gradient vector field $\boldsymbol{\nabla}\zeta(\boldsymbol{x}, t)$. This in turn permits determination of the true scalar energy dissipation rate field $\boldsymbol{\nabla}\zeta \cdot \boldsymbol{\nabla}\zeta(\boldsymbol{x}, t)$. Examples of the resulting four-dimensional data for $\zeta(\boldsymbol{x}, t)$ and $\boldsymbol{\nabla}\zeta \cdot \boldsymbol{\nabla}\zeta(\boldsymbol{x}, t)$ were shown in Part 1; additional examples are given in Southerland & Dahm (1994, 1996).

Each four-dimensional measurement produces the scalar and dissipation field values at over three billion individual points throughout a small spatio-temporal region in the flow. This region consists of 256^2 points in each measurement plane, spanning two inner (viscous) lengthscales λ_ν and $\frac{1}{20}$ of the outer lengthscale δ in each direction, and six planes in the third spatial direction, and can accommodate up to 8000 points spanning 120 inner timescales (λ_ν^2/ν) and 2 outer timescales (δ/u) in the temporal direction. Thus, the largest scaling range is accessible in the temporal dimension, where 12 multiples of two in scales, corresponding to 4096-point data records, can be analysed. For this reason, the present study is based on examining the applicability of multifractal scale similarity in 4096-point temporal intersections through these $\zeta(\boldsymbol{x}, t)$ and $\boldsymbol{\nabla}\zeta \cdot \boldsymbol{\nabla}\zeta(\boldsymbol{x}, t)$ fields. Note that Taylor scale Reynolds numbers are $Re_\lambda \approx 41$, with outer scale Reynolds numbers $Re_\delta \approx 3000$ for these data.

The structure of velocity and scalar fields in turbulent shear flows at scales near and below λ_ν should be quasi-universal even for the present moderate Reynolds numbers, as evidenced by DNS studies of Jiménez *et al.* (1993). The Re_λ for the present data are well within the range of values over which the DNS results of Jiménez *et al.* showed Reynolds-number-independent collapse on inner variables of the fine-scale vortical structures of the flow. Moreover, high-wavenumber spatial scalar spectra from these same data (Southerland, Dahm & Dowling 1995) show the k^{-1} scaling predicted by Batchelor (1959) for large Sc mixing in turbulent flows. As a result, although the present measurements are from turbulent jets at a single Re_δ, the geometric scaling properties of the fine scales contained in them are believed to be largely representative of the scaling properties at the inner scales of all turbulent shear flows.

3. Multifractal concepts

Multifractal fields are created by the repeated application of a scale-invariant multiplicative process to an essentially arbitrary initial field. Such a multiplicative process, perhaps due to the continual stretching and folding of the conserved scalar field by the underlying time-varying strain rate and vorticity fields, is not implausible in a turbulent flow, with the required scale-invariance being naturally satisfied for scales sufficiently removed from any direct external influences. Among the simplest of such scale-invariant multiplicative processes is the random multiplicative mapping ('cascade'), in which a set of multipliers M that map the field from one iteration to the next is chosen at random from a prescribed distribution $P(M)$. After a sufficiently large number of such iterations, the precise details of the resulting field, say $\mu(\boldsymbol{x}, t)$, depend on the distribution $P(M)$ and the multiplicative mapping itself, but its scale-similarity properties will attain a universal form that is the central object of multifractal theory. As noted in §1, the primary interest is in the resulting fractal dimension $f(\alpha)$ of the

subset of $(\boldsymbol{x}, t)$ on which the singularities of various strengths α are concentrated in a set of measures $\mu_\epsilon(\boldsymbol{x}_i, t_i)$ derived from $\mu(\boldsymbol{x}, t)$.

To determine $f(\alpha)$ in practice, the field of interest $\mu(\boldsymbol{x}, t)$ is averaged over individual boxes of size ϵ centred at $(\boldsymbol{x}_i, t_i)$ to produce measures $\mu_\epsilon(\boldsymbol{x}_i, t_i)$ giving the fraction of the quantity within any given box as

$$\mu_\epsilon(\boldsymbol{x}_i, t_i) \equiv \frac{\langle \mu(\boldsymbol{x}, t) \rangle_\epsilon}{\langle \mu(\boldsymbol{x}, t) \rangle_L} \frac{\epsilon}{L}, \tag{1}$$

where L is the record length. The set of measures is then used to construct a set of partition functions

$$X_q(\epsilon) \equiv \sum_{i=1}^{N(\epsilon)} [\mu_\epsilon(\boldsymbol{x}_i, t_i)]^q, \tag{2}$$

where $N(\epsilon)$ is the total number of boxes of scale ϵ and q is any real number. Thus, for $q = 0$, $X_q(\epsilon)$ reduces to the box-counting technique of fractal analysis (see Part 1), while for other q values, a weighted box-counting occurs. Indeed, just as in fractal analysis, it is the scaling of $X_q(\epsilon)$ with ϵ that is of central interest, with scale similarity for any q yielding a power law scaling as

$$X_q(\epsilon) \sim \epsilon^{\tau(q)}. \tag{3}$$

Thus, the $X_q(\epsilon)$ provide one means to assess the applicability of multifractal scale similarity.

The exponents $\tau(q)$ in the power-law scalings in (3), if they exist, can be related to $f(\alpha)$ as

$$\alpha(q) = \frac{\partial}{\partial q} \tau(q), \tag{4a}$$

$$f(\alpha(q)) = q\alpha(q) - \tau(q). \tag{4b}$$

Alternatively, they can be equivalently expressed in the generalized Renyi dimensions D_q (Hentschel & Procaccia 1983) as

$$D_q = \tau(q)/(q-1). \tag{5}$$

In terms of local singularity strengths, if $\mu(\boldsymbol{x}, t)$ has a power-law scaling at $\boldsymbol{x}'$ of the form $\mu(\boldsymbol{x}) \sim |\boldsymbol{x} - \boldsymbol{x}'|^{\alpha-1}$, with $\alpha > 0$, then from (1) the resulting measure $\mu_\epsilon(\boldsymbol{x}') \sim \epsilon^\alpha$ is said to have a singularity of strength α in ϵ at $\boldsymbol{x}'$. If all points with the same α form a set with fractal dimension $f(\alpha)$, then from (2) and (3) the relations between $\tau(q)$ and $f(\alpha)$ in (4) follow readily. It should be noted that this physical interpretation of $f(\alpha)$ as the dimension of the set of points with singularity strength α can fail under certain circumstances. It appears to be correct for invariant hyperbolic sets (Bohr & Rand 1987; Collet, Lebowitz & Porzio 1987) but Ott, Grebogi & Yorke (1989) suggest that for non-hyperbolic attractors it may hold only over a limited range of α values. Detailed treatments of the multifractal formalism are given by Falconer (1990) and Pietgen, Jurgen & Saupe (1992).

4. Multifractal scale-similarity criteria

Assessment of the applicability of these multifractal scale-similarity concepts to experimental data from turbulent flows requires a criterion for discerning fields with genuine multifractal scaling from those that have some other type of similarity. This

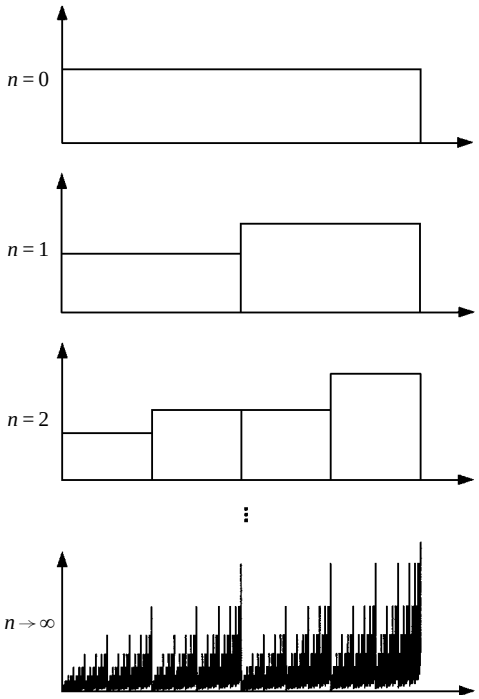

FIGURE 1. An example of the construction of a binomial set with $m = 0.4$. The highly intermittent nature of the set becomes apparent as $n \to \infty$. The non-random nature of this set, however, makes it a poor surrogate for turbulent fields.

section evaluates the reliability of various potential means for identifying multifractal scale similarity in data records of finite length, and develops strict criteria that allow reliable discrimination between multifractal and non-multifractal fields.

4.1. *Partition functions $X_q(\epsilon)$ and scaling exponents $\tau(q)$*

The most direct criterion for assessing the applicability of multifractal scale similarity in any given field $\mu(\boldsymbol{x}, t)$ is the requirement for power-law scaling in the $X_q(\epsilon)$ in (3), and thus for linear scaling in $\log X_q(\epsilon)$ versus $\log(\epsilon/L)$. Analogous with Parts 1 and 2, the linearity necessary to judge rigorously any given field either to be or not to be multifractal can be determined from the $X_q(\epsilon)$ scaling demonstrated by known multifractal gauge fields having the same record lengths as the present data. Such multifractal gauge fields can be readily constructed in one dimension from the repeated application, either deterministically or stochastically, of a scale-similar multiplicative process.

Among deterministically scale-similar gauge fields, the simplest are those generated by the classical binomial multiplicative process. At each stage of the construction, the 'mass' contained in any given cell is distributed over two cells, each of which is half the size of the previous stage, with fraction $M = m$ of the mass always going into the left-hand cell and $M = 1-m$ into the right-hand cell. For any choice of $m \neq 0.5$, the result of repeated application of this binomial process produces a highly intermittent field $\mu(x)$ after sufficiently many repetitions. This is shown in figure 1 for $m = 0.4$ after 12 repetitions, producing a record of length $N = 4096$ cells that matches the temporal record lengths of the experimental data in §2. This intermittent $\mu(x)$ can be analysed as in §3 to yield the partition functions $X_q(\epsilon)$ in (2). The resulting $\log X_q(\epsilon)$ *vs.* $\log(\epsilon/L)$

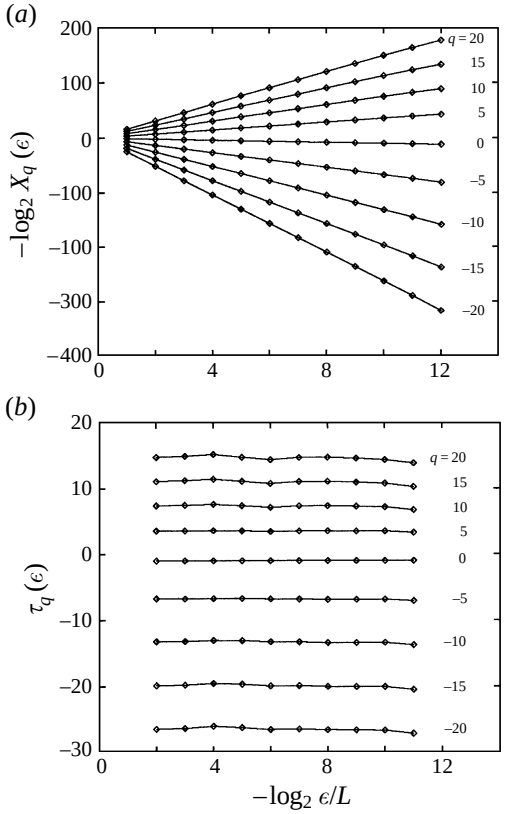

FIGURE 2. (*a*) The logarithm of the partition function $X_q(\epsilon)$ and (*b*) its derivative $\tau_q(\epsilon)$ obtained from analysis of the binomial set shown in figure 1. The linear scaling of $\log_2 X_q(\epsilon)$ *vs.* $-\log_2 \epsilon/L$ reflected in the scale independence of $\tau_q(\epsilon)$ indicates multifractal scaling.

from the choice of m in figure 1 are shown in figure 2(*a*) for $-20 \leqslant q \leqslant 20$. Note that these partition functions clearly demonstrate the linearity expected for such a multifractal field. The corresponding scaling exponents $\tau(q)$, obtained by differentiating at each scale ϵ/L in figure 2(*a*), are given in figure 2(*b*). These clearly show the scale independence for each q that is expected from the inherently multiplicative construction of $\mu(x)$.

The results in figure 2 are typical for deterministically scale-similar gauge fields $\mu(x)$ with record length $N = 4096$. However, as noted in Part 1, any scale similarity in turbulent flows is more likely to be stochastic than deterministic. It is thus necessary to establish standards analogous to those in figure 2 for the required linearity in $X_q(\epsilon)$ and scale independence in $\tau(q)$ applicable for stochastically scale-similar fields with the same record length. Such gauge fields can be readily generated by extending the procedure in figure 1 to a random multiplicative cascade process with a scale-independent multiplier distribution $P(M)$. As in figure 1, at each stage the mass in any given cell is again distributed over two cells, each half the size of the previous stage, but the mass multiplier M for each such division is now determined randomly from the scale-independent distribution $P(M)$. Choosing the bilinear distribution shown in figure 3(*a*) produced the intermittent $\mu(x)$ in figure 3(*b*) after 12 repetitions, again giving $N = 4096$. Note that, owing to the stochastic nature of the generation process, arbitrarily many different realizations $\mu(x)$ can be produced from the same $P(M)$. Each

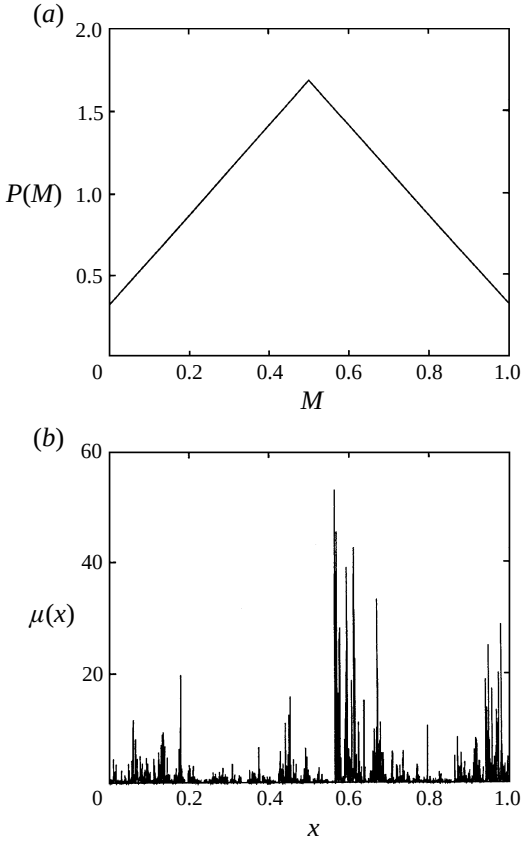

FIGURE 3. (*a*) The multiplier distribution $P(M)$ used in a random multiplicative cascade to produce the intermittent gauge field $\mu(x)$ shown in part (*b*).

such $\mu(x)$ differs in detail, but has the same underlying multiplicative scale-similarity properties. For the particular realization in figure 3(*b*), the resulting $\log X_q(\epsilon)$ versus $\log(\epsilon/L)$ are shown in figure 4(*a*), and the corresponding $\tau(q)$ are shown in figure 4(*b*). These should be compared with the corresponding results for the deterministically scale-similar gauge sets in figure 2.

It is immediately evident that, with finite-length records of stochastically scale-similar fields, the scale-independent $\tau(q)$ signature characteristically associated with multifractal fields is achieved only for relatively small $|q|$. This closely parallels results seen from the fractal analyses in Parts 1 and 2. In those cases, statistical convergence based on very large numbers of individual gauge set realizations was used to overcome this uncertainty. This was practical in the restricted dimensional space of the fractal analyses in Parts 1 and 2. However, an analogous approach for the present multifractal analyses is prohibitive owing to the increased variability for different q values in $X_q(\epsilon)$ and $\tau(q)$. As a consequence, for the present record lengths, a criterion based on linearity of $X_q(\epsilon)$ and scale independence of $\tau(q)$ alone does not appear to provide a meaningful way to test for multifractal scale similarity in data records from the turbulent flow measurements.

This becomes fully apparent when analogous results in figure 5 for a negative test case, namely $X_q(\epsilon)$ and $\tau(q)$ from manifestly non-multifractal gauge sets, are compared with those in figures 2 and 4. In this case, $\mu(x)$ is constructed from a lognormally

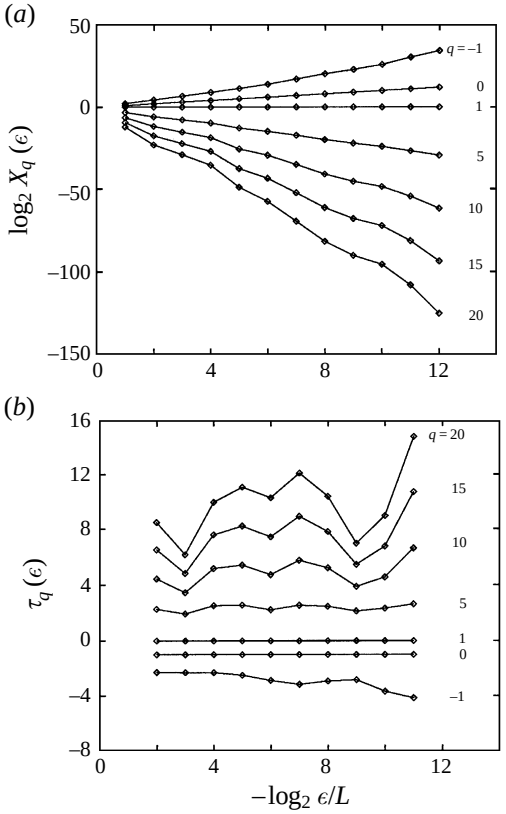

FIGURE 4. (*a*) The logarithm of the partition function $X_q(\epsilon)$ and (*b*) its scaling exponents $\tau(q)$ obtained from the multiplicative gauge field in figure 3(*b*). The stochastic nature of the multiplicative process leads to apparent scale dependencies in the scaling exponents $\tau(q)$, in contrast to the analogous results for deterministic multiplicative process in figure 2.

distributed random variable without any underlying scale-similar multiplicative process, again with record length $N = 4096$. The resulting partition functions and their scaling exponents in figures 5(*a*) and 5(*b*), respectively, show no clear means to objectively distinguish them from the corresponding results in figures 4(*a*) and 4(*b*) for the stochastically scale-similar gauge set, save for a statistical criterion that, as noted above, is computationally prohibitive in this study given the number of degrees of variability in $X_q(\epsilon)$ and $\tau(q)$. Accordingly we conclude that, for the present study, $X_q(\epsilon)$ and $\tau(q)$ cannot be reliably used to determine whether or not a given record with the present record length displays multifractal scale similarity.

4.2. *Dimensions $f(\alpha)$ and D_q*

For the same gauge sets $\mu(x)$ considered in §4.1, results for the dimensions $f(\alpha)$ and D_q are shown in figures 6–8. To obtain $f(\alpha)$ in (4) and D_q in (5), the $\tau(q)$ involved are from least-squares linear fits through the $X_q(\epsilon)$ results in figures 2(*a*), 4(*a*) and 5(*a*). The binomial multiplicative process in figure 1 and the random multiplicative cascade process with scale-independent bilinear multiplier distribution $P(M)$ in figure 3 allow analytical solutions for $f(\alpha)$ and D_q, which are shown for comparison. The results for the (deterministic) binomial multiplicative process in figure 6 are in relatively good agreement with the analytical solution. Note that in this case the interpretation of the α as singularity strengths in the $\mu(\boldsymbol{x}, t)$ field, and $f(\alpha)$ as the fractal dimensions of the

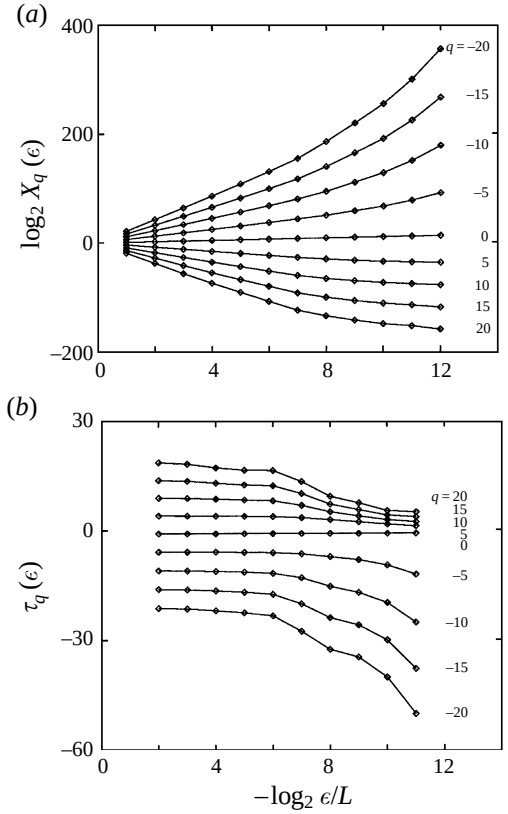

FIGURE 5. (*a*) The logarithm of the partition function $X_q(\epsilon)$ and (*b*) its scaling exponents $\tau(q)$ obtained from a lognormally distributed random gauge field.

sets on which they reside, appears reasonable since $0 < f(\alpha) \leqslant 1$. For $m < 0.5$, $f \to 0$ as $\alpha \to \alpha_{min} = -\log_2 (1-m) \approx 0.74$ occurring when $q \to +\infty$, and $\alpha \to \alpha_{max} = -\log_2 m \approx 1.32$ occurring when $q \to -\infty$.

The corresponding results for $f(\alpha)$ from the multiplicative cascade process in figure 7(*a*) appear to be in at least equally good agreement with the analytical result as for the binomial result in figure 6(*a*). This is somewhat surprising in view of the fact that the $\tau(q)$ results for these two fields in figures 2(*b*) and 4(*b*) appear to show very different agreement with the ideal of scale-invariant scaling exponents that are central to multifractal theory. Evidently, $f(\alpha)$ conveys little information about the requisite scale-independence of the scaling exponents $\tau(q)$. Equally important is that the physical interpretation of $f(\alpha)$ becomes more problematic in such cases, with negative dimensions occurring for many $P(M)$ distributions and $f(\alpha) \to -\infty$ as $\alpha \to 0$ and $\alpha \to \infty$. This hampers the description of $f(\alpha)$ as the dimension of the set of points with singularity strength α. The interpretation can be salvaged, however, through large deviation theory, where the method of intersections allows interpreting negative dimensions as intersections in a higher-dimensional space of an exceedingly sparse set (Mandelbrot 1990, 1991; Meneveau & Sreenivasan 1991). Similarly, the result in figure 7(*b*) shows D_q exceeding the support dimension $D_0 = 1$ for $q < 0$, with $D_q \to \infty$ as $q \to -1$.

The point is that none of these pathologies in $f(\alpha)$ or D_q can be viewed as criteria for rejecting a hypothesis of multifractal scale similarity in a given data record, since even

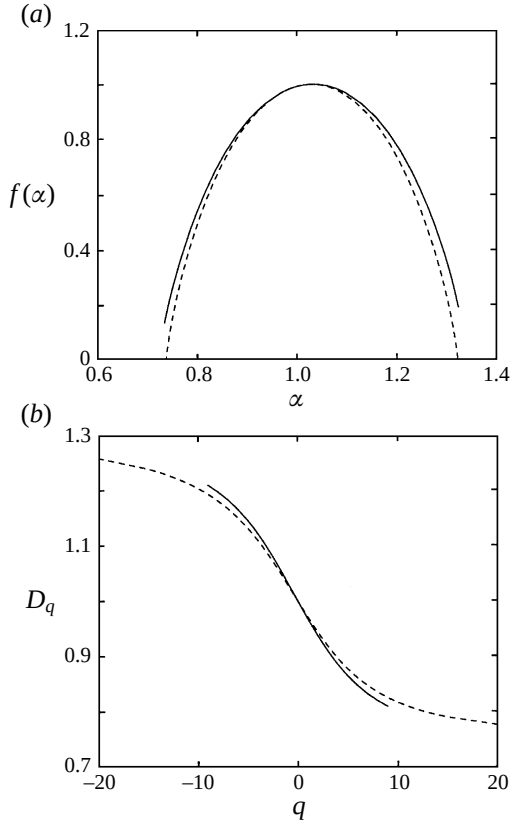

FIGURE 6. The dimensions (*a*) $f(\alpha)$ and (*b*) D_q from $\tau(q)$ shown in figure 2 for the deterministic binomial gauge set in figure 1. ——, numerical; – – –, exact.

manifestly multifractal gauge fields produced by genuine multiplicative cascade processes with scale-invariant multiplier distributions show these features. Moreover, these features have nothing to do with the numerical algorithm used to determine $f(\alpha)$ and D_q from $\mu(x)$, since they are present even in the analytical results for such gauge fields. As a consequence, $f(\alpha)$ and D_q alone do not appear to provide a meaningful way to test for multifractal scale similarity in data records from the turbulent flow measurements.

This again becomes completely apparent from results in figure 8, where $f(\alpha)$ and D_q are presented for the inherently non-multifractal lognormally distributed random field $\mu(x)$ constructed without any scale-similar multiplicative process, for which $X_q(\epsilon)$ and $\tau(q)$ were shown in figure 5. Both curves do not appear in any way obviously distinguishable from the corresponding results for multifractal gauge fields in figures 6 and 7. Accordingly, we conclude that, for the present study, while $f(\alpha)$ and D_q are of inherent interest they provide no means to assess the applicability of multifractal scale similarity.

4.3. *Multiplier distributions* $P(M_\epsilon)$

Owing to the inadequacy of $X_q(\epsilon)$ and $\tau(q)$ in §4.1 and $f(\alpha)$ and D_q in §4.2 for reliably discriminating between multifractal and non-multifractal fields $\mu(x)$, a further criterion based on scale invariance of the multiplier distribution $P(M)$, originally proposed by Sreenivasan (1991*b*) and Chhabra & Sreenivasan (1992), is examined. The field $\mu(x)$ is used to obtain a $P(M_\epsilon)$ distribution at each scale ϵ by effectively reversing the

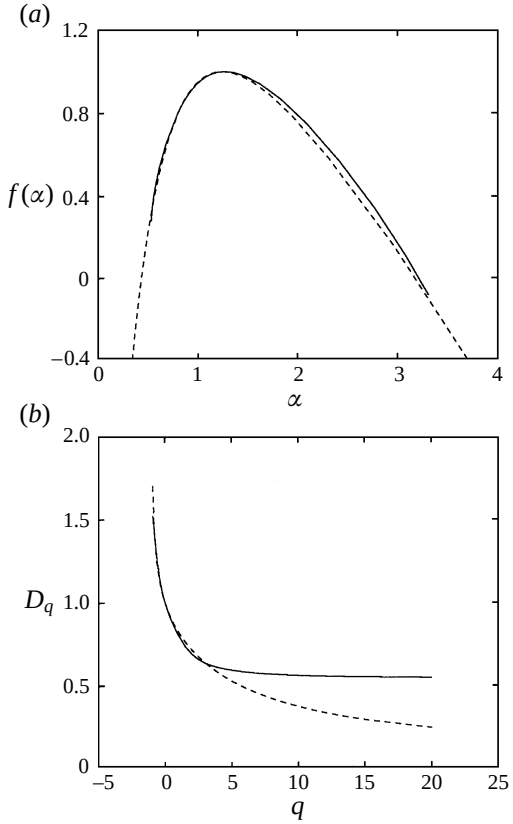

FIGURE 7. The dimensions (*a*) $f(\alpha)$ and (*b*) D_q from $\tau(q)$ in figure 4 for the multiplicative cascade shown in figure 3. ——, numerical; – – –, exact.

multiplicative process used to generate the multifractal gauge sets in §4.1. The multiplier M_ϵ between successive scales at any point $(\boldsymbol{x}_i, t_i)$ is thus determined as

$$M_\epsilon(\boldsymbol{x}_i, t_i) \equiv \frac{\displaystyle\int_{|\boldsymbol{x}-\boldsymbol{x}_i|<\epsilon/a}\int_{|t-t_i|<\epsilon/a} \mu(\boldsymbol{x}, t)\,\mathrm{d}\boldsymbol{x}\,\mathrm{d}t}{\displaystyle\int_{|\boldsymbol{x}-\boldsymbol{x}_i|<\epsilon}\int_{|t-t_i|<\epsilon} \mu(\boldsymbol{x}, t)\,\mathrm{d}\boldsymbol{x}\,\mathrm{d}t}, \tag{6}$$

where, for the present temporal intersections, the integrals extend over time only. If the field is multifractal, then $P(M_\epsilon)$ may, in general, be expected to show scale invariance, and its moments related to the scaling exponents $\tau(q)$, and hence to the dimensions $f(\alpha)$, as

$$\tau(q) = -D_0 - \log_a \langle M^q \rangle, \tag{7}$$

where D_0 is the support dimension and a is the number of subcells into which each cell is divided in the scale-similar mass division process (here $a = 2$).

For the binomial gauge set in figure 1, the original scale-invariant multiplier distribution $P(M)$ used to generate $\mu(x)$ consisted of delta functions at the multiplier values $M = 0.4$ and 0.6. When this $\mu(x)$ is decomposed into multiplier values via (6), the results obtained for $P(M_\epsilon)$ are shown in figure 9. Except at the smallest scales, the multiplier distributions obtained do not agree particularly well with the original $P(M)$ used to generate $\mu(x)$, but this is merely because the integration limits in (6), in general, do not coincide with the cell boundaries used in the multiplicative construction process

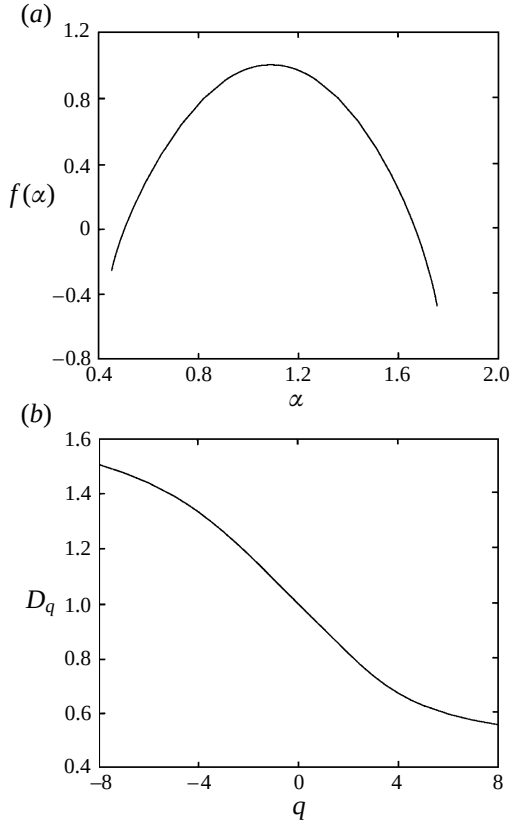

FIGURE 8. The dimensions (*a*) $f(\alpha)$ and (*b*) D_q from $\tau(q)$ in figure 5 for the lognormally distributed random gauge field.

for $\mu(x)$; if they do, then the correct $P(M)$ is exactly recovered. Moreover, as will be seen below, for most distributions this effect is small. Note also that the $P(M_\epsilon)$ are not completely scale-invariant. At very small scales, there are significant variations in the distributions obtained from (6), presumably due again to the effects of coincidence with cell boundaries. However, for a wide range of intermediate scales (spanning a range of 2^5 in lengthscales) the resulting $P(M_\epsilon)$ are virtually identical, as would be expected for a field generated by a scale-similar multiplicative process. Thus, the scale invariance of $P(M_\epsilon)$ over at least a limited range of scales provides a potential means for assessing multiplicative scale similarity.

Moreover, unlike $X_q(\epsilon)$ and $\tau(q)$ in §4.1, the scale similarity in the multiplier distributions $P(M_\epsilon)$ seen in figure 9 appears to be unaffected by the change from a deterministic to a stochastic character in the underlying multiplicative process. This can be seen in figure 10, where $P(M_\epsilon)$ distributions from (6) are shown for the $\mu(x)$ in figure 3 obtained from the random multiplicative cascade process with bilinear $P(M)$. At scales sufficiently large for the coincidence with cell boundaries to be negligible, the multiplier distributions obtained are essentially scale-invariant, and are in good agreement with the original bilinear distribution in figure 3(*a*). This is found for all stochastic multiplicative processes examined, and we conclude that a criterion based on scale invariance in $P(M_\epsilon)$ appears to provide a reliable means for assessing the applicability of multifractal scale similarity in experimental data with record lengths comparable to the present data.

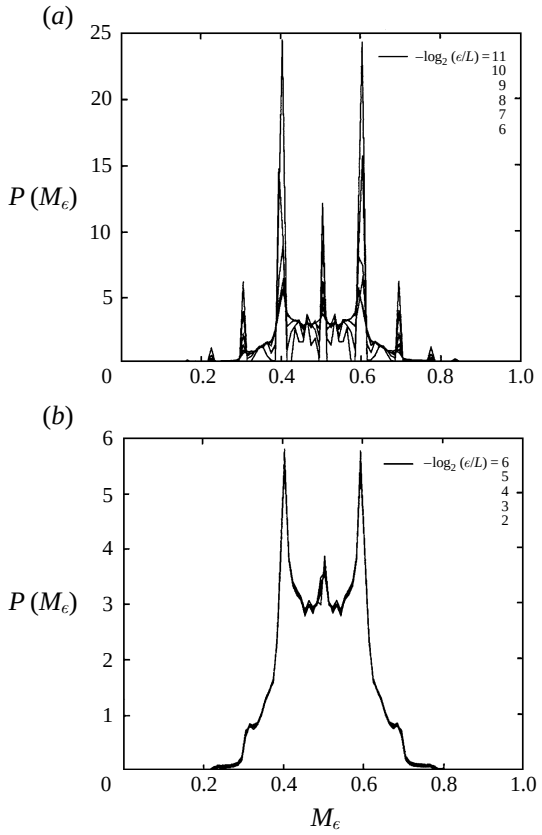

FIGURE 9. The multiplier distributions $P(M_\epsilon)$ from (6) for the binomial gauge field $\mu(x)$ in figure 1.

This is further supported by the lack of any scale invariance in the multiplier distributions $P(M_\epsilon)$ in figure 11 obtained from the random lognormal field $\mu(x)$ examined previously in figure 5 and 8, which has no underlying scale similarity. Note that, unlike the corresponding results for multifractal sets in figures 9 and 10, the $P(M_\epsilon)$ for the random set in figure 11 clearly do not show scale invariance over any range of scales. For random sets, as ϵ increases the μ_ϵ become increasingly accurate estimates of the average value of μ, and so the width of the peak in $P(M_\epsilon)$ near $M = 0.5$ is proportional to $\epsilon^{-1/2}$, and as a result $P(M_\epsilon)$ can never become scale invariant.

4.4. *The scale invariance criterion* $L_1(\epsilon)$

Based on the results in §§4.1–4.3, a criterion based on scale invariance in the multiplier distributions $P(M_\epsilon)$ appears to provide the only reliable means for accepting or rejecting the hypothesis of scale similarity in any given field $\mu(x)$. This section determines rigorous statistical bounds on the maximum allowable scale-to-scale variation in $P(M_\epsilon)$ for accepting or rejecting the hypothesis of multifractal scale similarity over any range of scales ϵ.

This is done by determining the L_1 difference norm between $\langle P(M_\epsilon)\rangle$ at successively smaller scales ϵ and $\frac{1}{2}\epsilon$ as

$$L_1(\epsilon) \equiv \int_0^1 |\langle P(M_\epsilon)\rangle - \langle P(M_{\epsilon/2})\rangle| \, \mathrm{d}M. \tag{8}$$

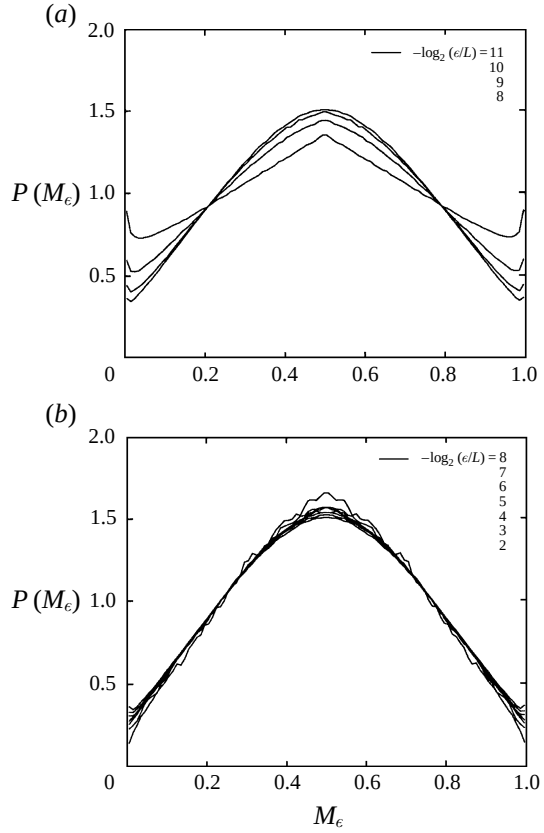

FIGURE 10. The multiplier distributions $P(M_\epsilon)$ obtained from (6) for 2000 individual realizations of gauge fields $\mu(x)$ generated by the multiplicative cascade process in figure 3. Note that over a wide range of scales, $P(M_\epsilon)$ in (b) agrees well with $P(M)$ in figure 3(a).

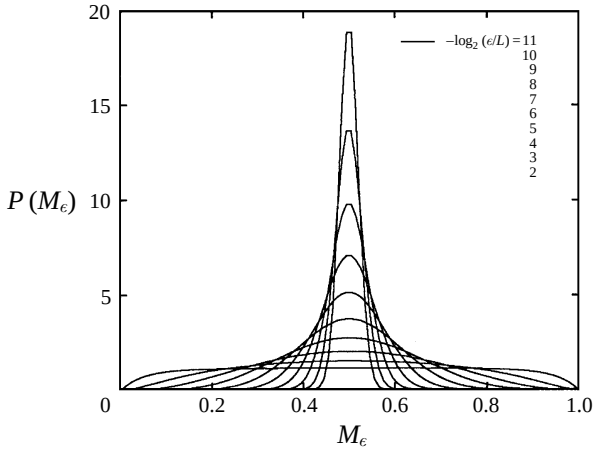

FIGURE 11. The multiplier distributions $P(M_\epsilon)$ obtained from (6) for 2000 individual realizations of non-multifractal gauge fields $\mu(x)$ generated by a lognormally distributed random variable. These results exhibit no scale invariant multiplier distributions over any range of scales.

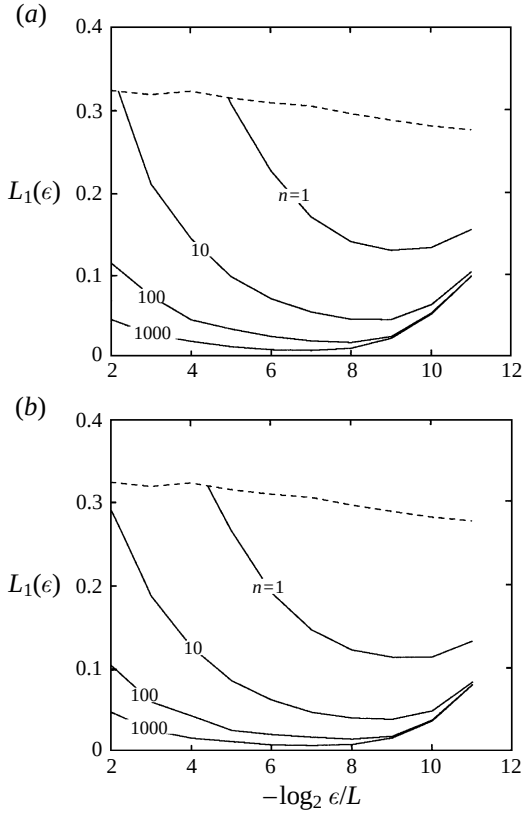

FIGURE 12. $L_1(\epsilon)$ from (8) quantifying differences between $\langle P(M_\epsilon)\rangle$ at successively smaller scales ϵ for gauge sets with $P(M)$ obtained from (*a*) the scalar dissipation field data, and (*b*) the scalar field data. Results are shown for varying numbers n of independent realizations of multifractal gauge sets (——) and random log normal gauge sets (– – –).

The average multiplier distributions are obtained from (6) over n independent realizations of scale-similar gauge fields $\mu(x)$ generated by a multiplicative process with the same $P(M)$. The resulting $L_1(\epsilon)$ difference norm values will thus depend on the choice of $P(M)$ used to generate the gauge fields, on the total number n of individual realizations of the gauge field, and on the record length of the gauge fields. The latter is addressed by using gauge sets having the same 4096-cell record length as the experimental data. The former is addressed by computing $L_1(\epsilon)$ for gauge fields constructed with multiplier distributions $P(M)$ obtained directly from each type of data being analysed.

Thus figure 12(*a*) shows the resulting $L_1(\epsilon)$ for various n when $P(M)$ is set to the multiplier distribution obtained from the measured scalar dissipation field values (see figure 18*b*). These curves provide the standard for assessing the hypothesis of multifractal scale similarity in any n independent records from the scalar dissipation field data $\nabla\zeta\cdot\nabla\zeta(\boldsymbol{x}, t)$. Similarly, figure 12(*b*) shows the slightly different $L_1(\epsilon)$ that result for the $P(M)$ obtained from the measured conserved scalar field values (see figure 19*b*), and provides the test for the hypothesis of multifractal scale similarity in any n independent records from the conserved scalar field data $\zeta(\boldsymbol{x}, t)$. Also shown for comparison in both cases is the $L_1(\epsilon)$ that results from the random lognormal field $\mu(x)$ in figure 11.

Finally, note that, as n increases, the scale-to-scale variation $L_1(\epsilon)$ in $\langle P(M_\epsilon)\rangle$

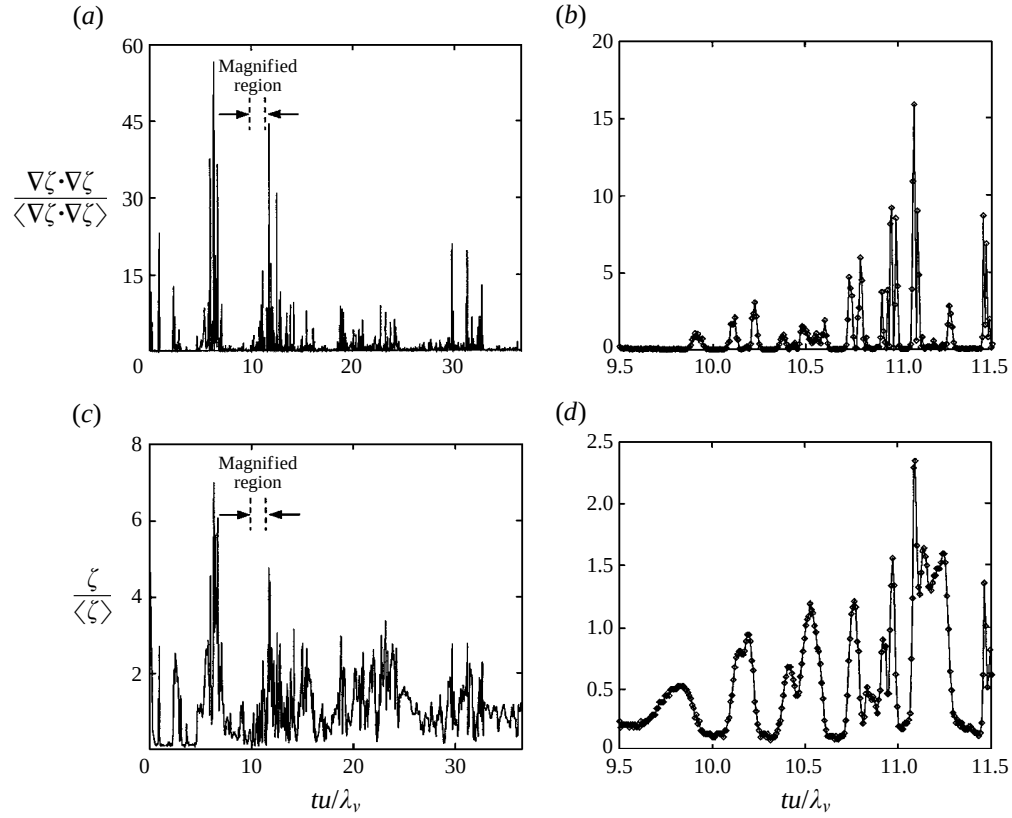

FIGURE 13. (*a*, *b*) Time series measurements of the scalar energy dissipation rate field $\nabla\zeta\cdot\nabla\zeta(\boldsymbol{x}, t)$ and (*c*, *d*) scalar field $\zeta(\boldsymbol{x}, t)$ obtained from a fully resolved four-dimensional data volume. (*a*, *c*) show the entire duration of the measurement while (*b*, *d*) contain magnified sections demonstrating the high temporal resolution achieved. Note the intermittent nature of the scalar energy dissipation rate field.

decreases owing to statistical convergence, however, $L_1(\epsilon)$ will not go to zero as $n\rightarrow\infty$. This is a result of the finite record length of each of the gauge fields, and thus is most apparent at the smallest analysis scales (i.e. toward the right-hand edge of each panel in figure 12). On the other hand, the increase in $L_1(\epsilon)$ at large scales is due to the smaller number of independent multipliers M_ϵ from (6) that can be obtained with increasing scale size ϵ in any finite length record. This effect can be offset by increasing the number n of independent records over which $\langle P(M_\epsilon)\rangle$, and hence $L_1(\epsilon)$, is computed.

5. Results for $\zeta(\boldsymbol{x}, t)$ and $\nabla\zeta\cdot\nabla\zeta(\boldsymbol{x}, t)$

Multifractal scale-similarity analyses of the type in §4 were conducted on nearly 2000 temporal intersections, each with 4096-point record lengths, through the data in §2 for the conserved scalar field $\zeta(\boldsymbol{x}, t)$, and on the same nearly 2000 intersections through the scalar energy dissipation rate field data $\nabla\zeta\cdot\nabla\zeta(\boldsymbol{x}, t)$. An example of a typical intersection through each of these fields is shown in figure 13. The scalar dissipation field in figure 13(*a*) can be compared, for example, with the intermittent $\mu(x)$ fields resulting from the deterministic and stochastic scale-similar multiplicative processes in figures 1 and 3(*b*).

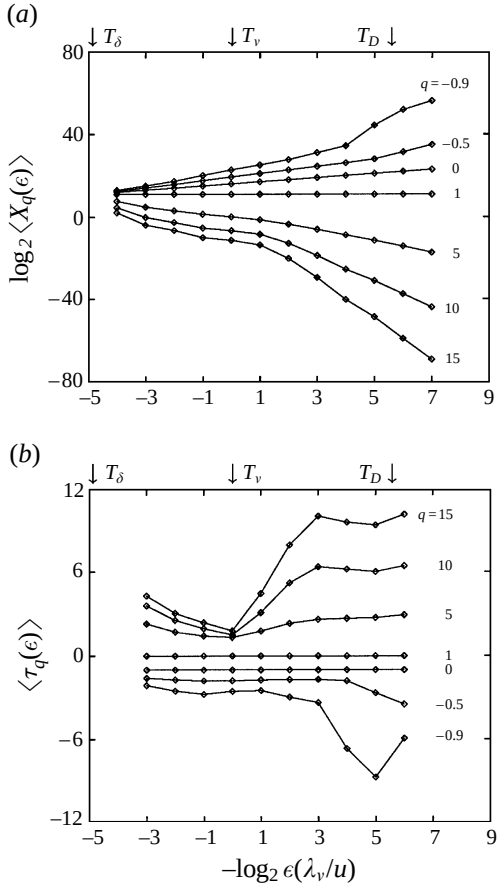

FIGURE 14. (*a*) The logarithm of the partition function $X_q(\epsilon)$ and (*b*) its scaling exponents $\tau(q)$ obtained from analyses of nearly 2000 temporal intersections through the scalar energy dissipation rate data $\boldsymbol{\nabla}\zeta\cdot\boldsymbol{\nabla}\zeta(\boldsymbol{x},t)$.

5.1. *Partition functions $X_q(\epsilon)$ and scaling exponents $\tau(q)$*

Each individual intersection produces a set of partition functions $X_q(\epsilon)$. The average of these nearly 2000 partition functions, $\log\langle X_q(\epsilon)\rangle$, that results from the dissipation field intersections is shown in figure 14(*a*), with the corresponding $\langle X_q(\epsilon)\rangle$ from the scalar field intersections shown in figure 15(*a*). These $\log\langle X_q(\epsilon)\rangle$ curves were differentiated to obtain the average scaling exponents $\langle\tau(q)\rangle$ shown in figures 14(*b*) and 15(*b*). The results in figures 14 and 15 can be compared with those in figure 2 for the deterministic scale-similar binomial gauge field, in figure 4 for the random multiplicative gauge field, and in figure 5 for the random log-normal variable. Although the results for $\zeta(\boldsymbol{x},t)$ in figure 15 show more nearly linear $\log\langle X_q(\epsilon)\rangle$ curves, and thus scaling exponents $\langle\tau(q)\rangle$ that are more nearly scale independent, than do the results in figure 14 for $\boldsymbol{\nabla}\zeta\cdot\boldsymbol{\nabla}\zeta(\boldsymbol{x},t)$, as was noted in §4.1 while these features are characteristic of multifractals they are not good criteria for accepting or rejecting the hypothesis that a given 4096-point data record displays multifractal scale similarity. Indeed, the results in figure 5 for the non-multifractal gauge field show roughly equally linear $\log X_q(\epsilon)$ and constant $\tau(q)$ as the results for the genuinely multifractal gauge field in figure 4.

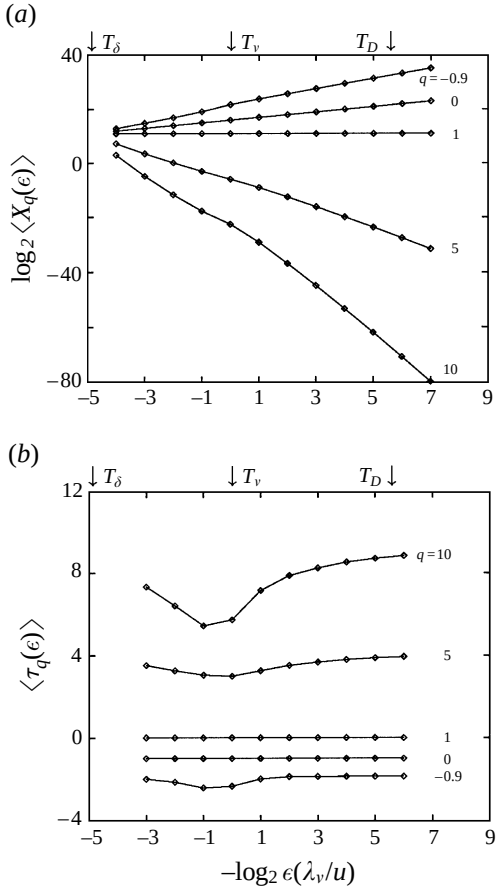

FIGURE 15. (*a*) The logarithm of the partition function $X_q(\epsilon)$ and (*b*) its scaling exponents $\tau(q)$ obtained from analyses of nearly 2000 temporal intersections through the conserved scalar data $\zeta(\boldsymbol{x}, t)$.

5.2. *Dimensions $f(\alpha)$ and D_q*

The $\tau(q)$ from least-squares fits in figures 14(*b*) and 15(*b*), over the range of ϵ where §5.3 indicates scale-similarity, yield the results in figures 16 and 17 for the dimensions $f(\alpha)$ and D_q via (4*a*, *b*). These $f(\alpha)$ and D_q curves have a similar form as the results for the multiplicative cascade process in figure 7, with a long tail of negative $f(\alpha)$ values for relatively large α, and no moments D_q for $q < -1$. However, as noted in §4.1, while this makes the physical interpretation of $f(\alpha)$ more problematic, it provides no grounds for rejecting (or accepting) the hypothesis that these data records display multifractal scale similarity.

5.3. *Multiplier distributions $P(M_\epsilon)$*

Figures 18 and 19 show the results obtained for the average multiplier distributions $\langle P(M_\epsilon) \rangle$ from (6) for the same nearly 2000 intersections with $\zeta(\boldsymbol{x}, t)$ and $\boldsymbol{\nabla}\zeta \cdot \boldsymbol{\nabla}\zeta(\boldsymbol{x}, t)$. The distributions in figure 18 give a clear indication of a scale similar multiplicative process underlying the scalar dissipation rate field $\boldsymbol{\nabla}\zeta \cdot \boldsymbol{\nabla}\zeta(\boldsymbol{x}, t)$. Note that figure 18(*b*) shows virtually identical multiplier distributions over a range of at least 2^5 in scale, spanning from $1.4\,\lambda_D/u \leqslant \epsilon \leqslant 1.0\,\lambda_\nu/u$. This range is essentially the same as that over

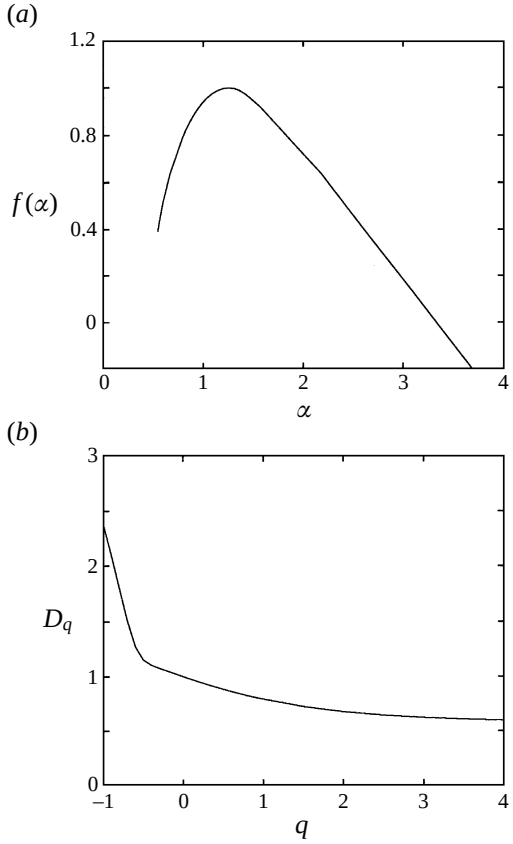

FIGURE 16. (*a*) The dimensions $f(\alpha)$ and (*b*) D_q obtained from $\tau(q)$ in figure 14 for the scalar energy dissipation rate field $\boldsymbol{\nabla}\zeta\cdot\boldsymbol{\nabla}\zeta(\boldsymbol{x},t)$.

which the multifractal gauge set in figure 10, generated by the scale-similar multiplicative process with the bilinear $P(M)$ in figure 3, also showed scale-independent multiplier distributions $P(M_\epsilon)$. Indeed, the multiplier distributions are found to be very nearly bilinear, in apparent agreement with previous measurements of Sreenivasan (1991*b*) and Chhabra & Sreenivasan (1992) for the kinetic energy dissipation surrogate $(\partial u/\partial t)^2$. The peaks in $\langle P(M_\epsilon)\rangle$ at scales $\epsilon < 1.4\,\lambda_D/u$ in figure 18(*a*) are most probably due to the influence of the diffusive cutoff process at these scales (see Part 2). At scales $\epsilon > 1.0\,\lambda_\nu/u$, figure 18(*a*) shows departures from the scale-similar $\langle P(M_\epsilon)\rangle$ in figure 18(*b*), but if a random multiplicative process were terminated at this scale, then the multiplier distribution at larger scales should quickly collapse to $M_\epsilon = 0.5$, as was seen in figure 11. However, the results in figure 18(*a*) show only a very slow approach to this value, indicating that there may be scale-similar dynamics even at scales above $1.0\,\lambda_\nu/u$. This will be clarified in §5.5.

The corresponding multiplier distributions $\langle P(M_\epsilon)\rangle$ in figure 19 for $\zeta(\boldsymbol{x},t)$ show some similarities with those for $\boldsymbol{\nabla}\zeta\cdot\boldsymbol{\nabla}\zeta(\boldsymbol{x},t)$ in figure 18, but there are important differences. The range of scales over which figure 19(*b*) shows a scale-independent distribution spans only a factor of at least 2^3, ranging from $0.5\,\lambda_\nu/u \leqslant \epsilon \leqslant \lambda_\nu/u$. Note also that the shape of the multiplier distribution over this range of scales is fundamentally different from the bilinear form in figure 18(*b*). More importantly, for scales $\epsilon < 0.5\,\lambda_\nu/u$, figure 19(*a*) shows that in this case $\langle P(M_\epsilon)\rangle$ rapidly departs from

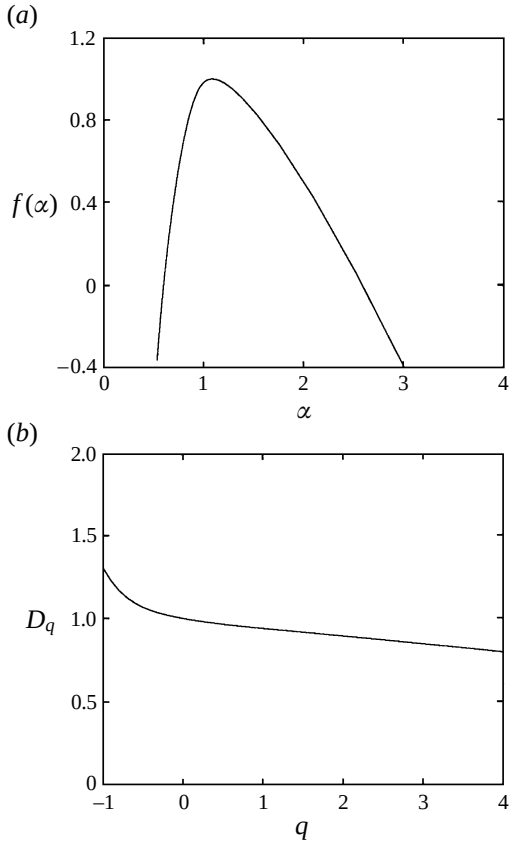

FIGURE 17. (*a*) The dimensions $f(\alpha)$ and (*b*) D_q obtained from $\tau(q)$ in figure 14 for the conserved scalar field $\zeta(\boldsymbol{x}, t)$.

the scale-similar form in figure 19(*b*) and collapses to the value $M_\epsilon = 0.5$. However, this collapse is for a different reason to that in figure 11. In the scalar field, at sufficiently small scales the values in adjacent cells become nearly the same owing to the dominant influence of the molecular diffusion process at those scales.

5.4. *The scale invariance criterion* $L_1(\epsilon)$

Figure 20 shows the $L_1(\epsilon)$ values obtained by comparing the scale-to-scale differences in the $\langle P(M_\epsilon)\rangle$ results of figures 18 and 19. Results for the scalar dissipation rate field $\boldsymbol{\nabla}\zeta\cdot\boldsymbol{\nabla}\zeta(\boldsymbol{x}, t)$ are shown in figure 20(*a*), where the corresponding threshold criteria from §4.4 for n fully independent multifractal gauge fields generated from a scale-invariant $P(M)$ are shown for comparison. Note that the multiplier distribution $P(M)$ used to generate each of the n multifractal gauge fields was that in figure 18(*b*). Also shown is the corresponding curve for the random lognormal set, which has no underlying scale-similarity.

It is apparent that the $L_1(\epsilon)$ values for the dissipation field in figure 20(*a*) are distinctly different from the results for the random lognormal set. They follow roughly the same trend as do the curves for the multifractal gauge fields, but do not approach the threshold curve for $n = 2000$. This is due to the correlated nature of the intersections. Although there are nearly 2000 intersections used in the analysis, they all are temporal intersections at slightly different spatial locations through the same four-

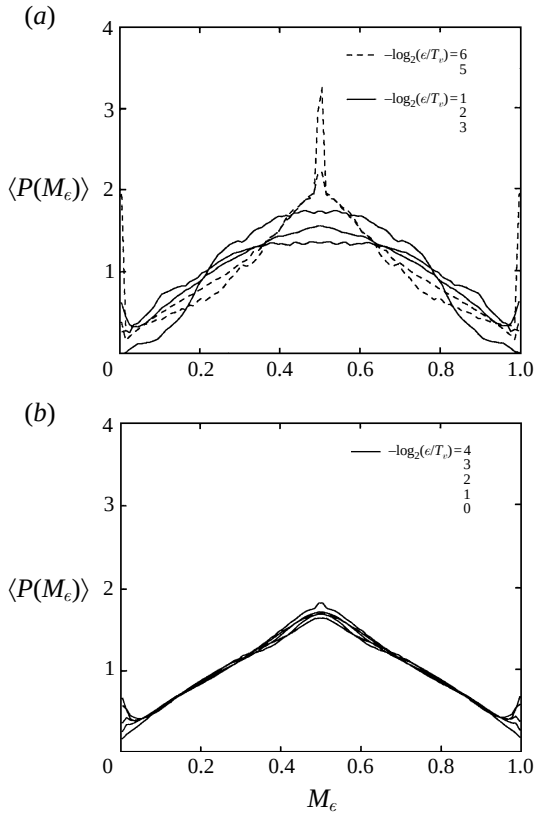

FIGURE 18. The multiplier distributions $\langle P(M_\epsilon)\rangle$ from (6) obtained from analyses of nearly 2000 temporal intersections through the scalar energy dissipation rate data $\nabla\zeta\cdot\nabla\zeta(\boldsymbol{x},t)$. Note that (*b*) shows the results over scales from $-\log_2\epsilon/T_\nu = 0,\ldots,4$ while (*a*) shows the results from smaller and larger scales.

dimensional data set $\boldsymbol{\nabla}\zeta\cdot\boldsymbol{\nabla}\zeta(\boldsymbol{x},t)$. As a consequence, all are correlated to varying degrees, with the result being to render the number of effectively independent intersections in the $\langle P(M_\epsilon)\rangle$ calculations dependent on the scale ϵ. This will be accounted for in § 5.5. The largest departure from the shape of the $L_1(\epsilon)$ curves for the multifractal gauge fields is seen at the largest scales, where the effect of the correlation is strongest and thus the effective number of independent intersections is smallest. At very small scales, the $L_1(\epsilon)$ result from the dissipation field data also departs significantly from the curves for the multifractal gauge fields, but this is to be expected since the diffusive cutoff will become significant as $\epsilon\to\lambda_D/u$. There is, moreover, a noticeable 'bump' at $\epsilon\approx 0.25\,\lambda_\nu/u$ in the local $L_1(\epsilon)$ curve from the dissipation field data that could potentially reflect the non-fractal inclusions of roughly the same scale found in Part 2 to be associated with the signature of the diffusive cutoff in the dissipation field.

The corresponding $L_1(\epsilon)$ curve from the conserved scalar field data $\zeta(\boldsymbol{x},t)$ is shown in figure 20(*b*), where the multiplier distribution $P(M)$ used to generate each of the n multifractal gauge fields is from figure 19(*b*). As was already suggested by the multiplier distributions in § 5.3, the scalar field apparently displays very different scale-similarity properties over this range of scales compared to those of the dissipation field in figure 20(*a*). While the shape of the curve at relatively large scales in figure 20(*b*) is

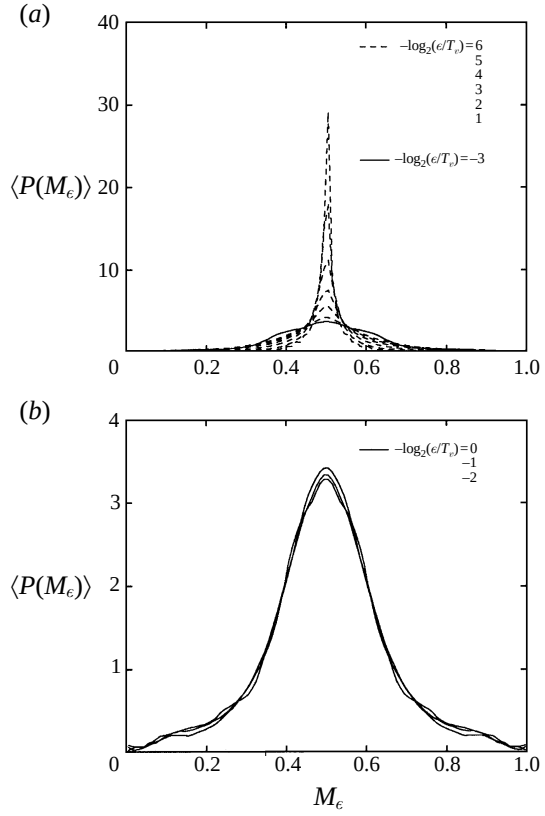

FIGURE 19. The multiplier distributions $\langle P(M_\epsilon)\rangle$ from (6) obtained from analyses of nearly 2000 temporal intersections through the conserved scalar data $\zeta(\boldsymbol{x}, t)$. Note that (*b*) shows the results over scales from $-\log_2 \epsilon/T_\nu = -2, \ldots, 0$ while (*a*) shows the results from smaller and larger scales.

similar to that for the dissipation field, this is influenced strongly by the reduction in correlation with scale ϵ. That effect will be addressed in §5.5. However, with decreasing ϵ the $L_1(\epsilon)$ curve from the scalar field data becomes fundamentally different from that for the dissipation field data as well as those from the multifractal gauge fields. This suggests that, at least for $\epsilon < 0.5\,\lambda_\nu/u$, the conserved scalar field does not display multifractal scale similarity. That conclusion will be seen from §5.5 as well, and furthermore appears consistent with the findings from Part 2.

5.5. *Effect of correlations on* $L_1(\epsilon)$

Since all of the nearly 2000 temporal intersections through each of the $\zeta(\boldsymbol{x}, t)$ and $\boldsymbol{\nabla}\zeta\cdot\boldsymbol{\nabla}\zeta(\boldsymbol{x}, t)$ fields considered in §5.4 are from the same four-dimensional data set at slightly different spatial locations, all are correlated to varying degrees. Thus, the number n of effectively independent intersections is significantly smaller. Moreover, the degree of correlation in the multipliers M_ϵ obtained from these intersections via (6) depends on ϵ. Thus the effective number of independent intersections will increase with decreasing ϵ, and this appears consistent with the $L_1(\epsilon)$ results in figure 20(*a*, *b*) (but not with the different forms of $L_1(\epsilon)$ from the scalar and dissipation field data for $\epsilon < 2\,\lambda_\nu/u$).

This effect can be corrected for by measuring how strongly correlated the multipliers M_ϵ are at each scale ϵ for any two intersections separated by a distance r. The resulting

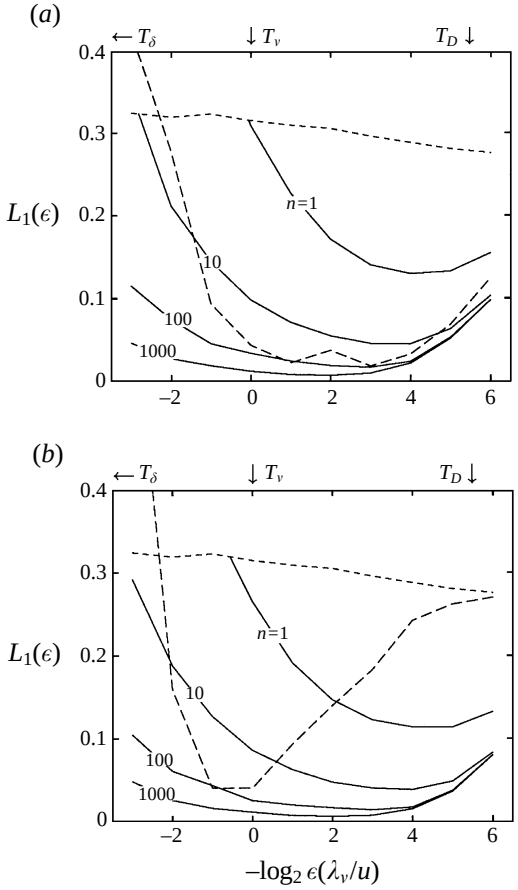

FIGURE 20. $L_1(\epsilon)$ from (8) for $\langle P(M_\epsilon)\rangle$ multiplier distributions from (*a*) the scalar dissipation field data in figure 18 (– – –), and (*b*) the scalar field data in figure 19 (– – –). Also shown are results from figure 12 for varying numbers n of independent realizations of multifractal gauge sets (——) and random lognormal gauge sets (– – –).

correlations $\rho_M(r;\epsilon)$ are shown in figure 21 for both the conserved scalar field data and the dissipation field data. Note that the variation in the multiplier correlations with ϵ is different for the two fields. In the dissipation field, the correlations strictly increase as ϵ increases, as might be expected. However, in the scalar field, the correlation of multipliers is considerable at the smallest ϵ and then decreases to a minimum at $\epsilon \approx \lambda_\nu/u$ before again increasing. This may provide information for extending random multiplicative cascades to higher-dimensional models of turbulence fields. For the present purposes, however, these correlations show that in both fields over the entire range of ϵ only about six effectively independent intersections can be obtained.

The $L_1(\epsilon)$ criteria from §4.4 can thus be recomputed with this much smaller number of independent intersections accessible by the data. The multiplier distributions $P(M)$ used to generate the multifractal gauge fields are once again taken from figures 18(*b*) and 19(*b*), with the resulting criteria shown in figure 22. Also shown in these figures are the $L_1(\epsilon)$ values for the dissipation field and the conserved scalar field, and for the random lognormal field.

It is readily apparent from the result in figure 22(*a*) that the dissipation field clearly obeys multifractal scale similarity for all scales $\epsilon > 0.03\,\lambda_\nu/u$ (and since $Sc \approx 2000$ in the present data this corresponds to $\epsilon > 1.4\,\lambda_D/u$). Whether it is the viscous scale or the

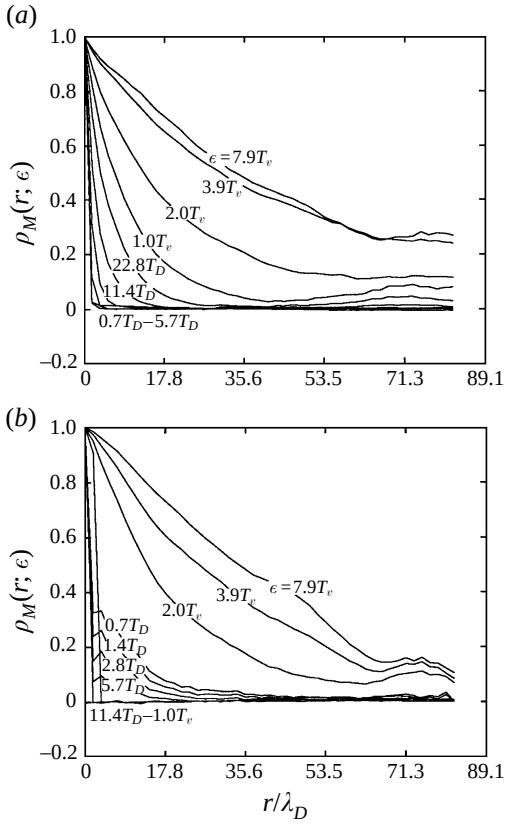

FIGURE 21. The correlation ρ as a function of r, the separation distance, between $M_\epsilon(t)$ for the nearly 2000 temporal intersections through (*a*) the scalar dissipation field data $\boldsymbol{\nabla}\zeta\cdot\boldsymbol{\nabla}\zeta(\boldsymbol{x},t)$ and (*b*) the conserved scalar field data $\zeta(\boldsymbol{x},t)$.

scalar diffusion scale that sets the scaling cutoff is not obvious, and would require comparable measurements at different Sc. Irrespective of this, the principal result from figure 22(*a*) is that the scalar energy dissipation field in turbulent flows displays a scale-invariant similarity consistent with a multiplicative cascade process that can be modelled with the bilinear multiplier distribution in figure 18(*b*).

It is also apparent from figure 22(*b*) that the conserved scalar field clearly does not follow any multifractal scale similarity consistent with a multiplicative cascade process at scales below $\epsilon < 0.5\,\lambda_\nu/u$. At larger scales, there is some indication of a possible scale-invariant similarity of this type in figure 22(*b*). However, the limited range of scales accessible by the present measurements precludes equally strong conclusions from being drawn for this range of scales. Nevertheless, the primary result from figure 22(*b*) is that while the scalar dissipation field is clearly multifractal at the small scales, the conserved scalar field is clearly not.

6. Discussion and conclusions

The results above were based on strict criteria for determining the applicability of multifractal scale similarity of the type produced by scale-invariant multiplicative cascades for describing the scale similarity properties of turbulent flows. Standards for

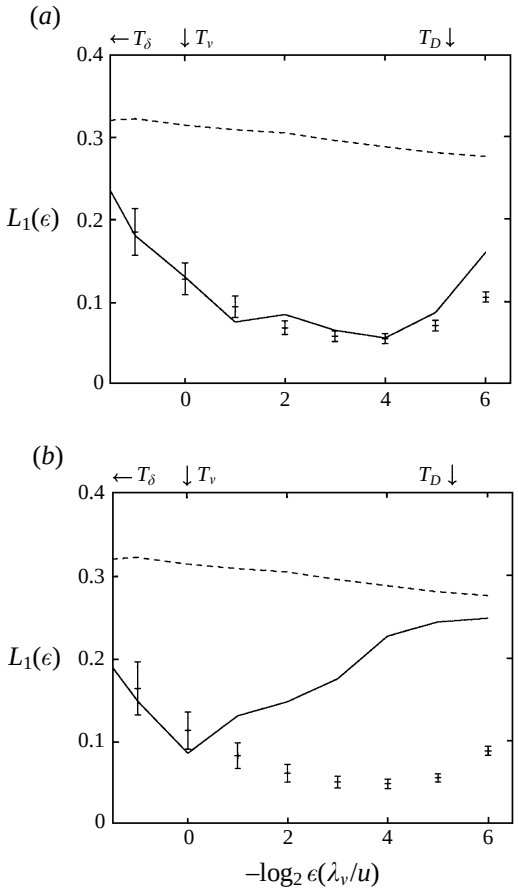

FIGURE 22. The $L_1(\epsilon)$ results for ——, (*a*) the scalar dissipation field $\boldsymbol{\nabla}\zeta \cdot \boldsymbol{\nabla}\zeta(\boldsymbol{x}, t)$ and (*b*) the conserved scalar field $\zeta(\boldsymbol{x}, t)$ from the maximum number ($n = 6$) of uncorrelated temporal intersections indicated by figure 21. Error bars show the corresponding $L_1(\epsilon)$ from the same number of multifractal gauge fields. Also shown are – – –, the corresponding results for random log-normal fields.

assessing multifractal scaling in experimental data with relatively short record lengths were established from multifractal gauge fields having the same record length, and the suitability of various constructs for discriminating between multifractal and non-multifractal similarity were examined. With these standards, an ensemble of data records could be objectively analysed to determine if it displayed scale similarity that was 'as multifractal as a given class of gauge sets having the same record length.'

Classical features of multifractal fields, including the linearity of the partition functions $\log X_q(\epsilon)$ with scale $\log(\epsilon/L)$, and the corresponding scale-independence of their scaling exponents $\tau(q)$, were found to be satisfied for multifractal gauge fields generated by multiplicative cascades of the deterministic type (e.g. figure 2), but not by cascades of the stochastic type (e.g. figure 4). Similarly, various apparent pathologies in the dimensions $f(\alpha)$ and D_q found in fully random gauge fields (e.g. figure 8) were also found in the dimensions resulting from gauge fields produced by stochastic scale-similar multiplicative cascades (e.g. figure 7). Thus, none of these constructs provided any obvious means of distinguishing between multifractal and random sets. However, multiplier distributions $\langle P(M_\epsilon)\rangle$ from (6) were found to provide a sensitive test of scale-invariance (e.g. figures 9–11), with the resulting scale-dependence in the $L_1(\epsilon)$

norm in (8) characterizing the maximum allowable scale-to-scale differences in the multiplier distributions for multifractal fields (e.g. figure 12*a*, *b*).

These criteria were used to examine multifractal scale similarity in nearly 2000 individual 4096-point temporal intersections through conserved scalar field data $\zeta(\boldsymbol{x}, t)$ and true scalar energy dissipation rate field data $\nabla\zeta\cdot\nabla\zeta(\boldsymbol{x}, t)$ from fully-resolved four-dimensional spatio-temporal measurements of the type in §2. The $L_1(\epsilon)$ results in figure 22(*a*) for the dissipation field clearly showed multifractal scale similarity for scales larger than $0.03\ \lambda_\nu/u$, which for the present $Sc \approx 2000$ corresponds to scales larger than $1.4\ \lambda_D/u$. In other words, the dissipation field is multifractal down to essentially the scalar diffusive scale. On the other hand, the corresponding results in figure 22(*b*) clearly showed that the conserved scalar field does not show multifractal scaling for scales smaller than $0.5\ \lambda_\nu/u$. At larger scales, the present results do not exclude multifractal scaling in the conserved scalar field, and indeed show some indications of possible multifractal scale similarity, but the limited range of scales accessible by these data do not permit an unequivocal assessment at these scales.

The present finding of multifractal scaling in the scalar energy dissipation field appears to support earlier findings of Prasad *et al.* (1988) and Sreenivasan & Prasad (1989), who based their assessments on apparent linearity in $\log X_q(\epsilon)$ with scale $\log(\epsilon/L)$ and the corresponding scaling exponents $\tau(q)$. However, the shape of the dimension spectrum $f(\alpha)$ found in those studies appears to be fundamentally different from the result in figure 16(*a*). In particular, the long tail for large α found in the present result does not appear in their result (e.g. figure 19 of Sreenivasan 1991*a*), which instead more closely resembles the $f(\alpha)$ from the binomial set in figure 6. Accordingly, the dimensions D_q in figure 16(*b*) are also quite different from the corresponding result in figure 20 of Sreenivasan (1991*a*). Nevertheless, there are similarities in the present multiplier distributions $\langle P(M_\epsilon)\rangle$ in figure 18(*b*) and those of Chhabra & Sreenivasan (1992), with both showing nearly similar bilinear distributions for $a = 2$ in (6). Moreover, many of the present results for the scale similarity properties of the true scalar dissipation rate field $\boldsymbol{\nabla}\zeta\cdot\boldsymbol{\nabla}\zeta(\boldsymbol{x}, t)$ closely resemble analogous results for surrogates based on $(\partial u/\partial t)^2$ of the kinetic energy dissipation rate field (e.g. Sreenivasan 1991*a*; Meneveau & Sreenivasan 1991). The present results are also consistent with the findings in Parts 1 and 2 that the scalar dissipation rate field is concentrated on a support geometry that displays fractal scale similarity.

The scale invariance and bilinear form of the multiplier distributions $\langle P(M_\epsilon)\rangle$ in figure 18 provide the basis for a simple model of the scalar dissipation rate field in turbulent flows. In particular, a stochastic multiplicative scale-similar cascade with essentially this same bilinear distribution (see figure 3*a*) produces one-dimensional sets of the type in figure 3(*b*), which should be compared with typical one-dimensional intersections through the true scalar dissipation field, such as figure 13(*a*). To the extent that the multifractal scale similarity found in this study extends to the entire range of scales, the implication is that the resulting multifractal sets from this simple cascade model should be statistically indistinguishable from the true dissipation fields.

It is, of course, possible that at least some aspects of the results found here will still depend on the outer scale Reynolds number Re_δ. As noted in §2, the present Reynolds numbers are necessarily low to permit full resolution of all spatial and temporal scales in the conserved scalar field, and to permit simultaneous measurements over all three space dimensions and time. Similar measurements at significantly higher Reynolds numbers are not yet possible. However, the present data, with $Re_\lambda \approx 41$ and $Re_\delta \approx 3000$, appear to be at sufficiently high Reynolds numbers for most aspects of the scalar field structure to have become largely Re independent. This is supported by DNS

results of Jiménez *et al*. (1993), who find Reynolds-number-independent collapse on inner variables of the fine-scale structure of flows at values of Re_λ as low as 35, and by the demonstrated k^{-1} scaling in high-wavenumber spatial scalar spectra from these same data (Southerland & Dahm 1994, 1996). Moreover, results from Part 1 indicated that effects of noise in these measurements were sufficiently small to leave the scale-similarity properties of both the conserved scalar field and the scalar dissipation rate field essentially unaffected. As a result, we conclude that these results for the applicability of multifractal scale similarity to the scalar and dissipation fields in the present data are largely representative of the scaling properties at the inner scales of all turbulent shear flows.

The three- and four-dimensional scalar field data used in this study were obtained at Michigan as part of the doctoral dissertation work of Dr Kenneth B. Southerland, under support from the Air Force Office of Scientific Research (AFOSR) Airbreathing Combustion program under Grant No. AFOSR-89-0541 and the Turbulence Structure and Control program under Grant No. F49620-92-J-0025.

REFERENCES

Batchelor, G. K. 1959 Small-scale variation of convected quantities like temperature in a turbulent fluid. *J. Fluid Mech.* **5**, 113–139.

Benzi, R., Paladin, G., Parisi, G. & Vulpiani, A. 1984 On the multifractal nature of fully developed turbulence and chaotic systems. *J. Phys.* A: *Math. Nucl. Gen.* **17**, 3521–3531.

Bohr, T. & Rand, D. 1987 The entropy function for characteristic exponents. *Physica* D **25**, 387–398.

Chechetkin, V. R., Lutovinov, V. S. & Turygin, A. Y. 1990 Multifractal structure of fully developed hydrodynamic turbulence. II. Intermittency effects in the distribution of passive scalar impurities. *J. Stat. Phys.* **61**, 589–605.

Chhabra, A. B. & Sreenivasan, K. R. 1992 Scale invariant multiplier distributions in turbulence. *Phys. Rev. Lett.* **68**, 2762–2765.

Collet, P., Lebowitz, J. L. & Porzio, A. 1987 The dimension spectrum of some dynamical systems. *J. Stat. Phys.* **47**, 609–644.

Dahm, W. J. A., Southerland, K. B. & Buch, K. A. 1991 Direct, high-resolution, four-dimensional measurements of the fine scale structure of $Sc \gg 1$ molecular mixing in turbulent flows. *Phys. Fluids* A **3**, 1115–1127.

Falconer, K. 1990 *Fractal Geometry: Mathematical Foundations and Applications.* John Wiley.

Frederiksen, R. D., Dahm, W. J. A. & Dowling, D. R. 1996 Experimental assessment of fractal scale similarity in turbulent flows. Part 1. One-dimensional intersections. *J. Fluid Mech.* **327**, 35–72.

Frederiksen, R. D., Dahm, W. J. A. & Dowling, D. R. 1997 Experimental assessment of fractal scale similarity in turbulent flows. Part 2. Higher-dimensional intersections and non-fractal inclusions. *J. Fluid Mech.* **338**, 89–126.

Frisch, U. & Parisi, G. 1985 In *Turbulence and Predictability in Geophysical Fluid Mechanics and Climate Dynamics* (ed. M. Ghil, R. Benzi & G. Parisi). North-Holland.

Frisch, U., Sulem, P. & Nelkin, M. 1978 A simple dynamical model of intermittent fully developed turbulence. *J. Fluid Mech.* **87**, 719–736.

Halsey, T. C., Jensen, M. H., Kadanoff, L. P., Procaccia, I. & Shraiman, B. I. 1986 Fractal measures and their singularities: The characterization of strange sets. *Phys. Rev.* A **33**, 1141–1151.

Hentschel, H. G. E. & Procaccia, I. 1983 The infinite number of generalized dimensions of fractals and strange attractors. *Physica* D **8**, 435–444.

Jiménez, J., Wray, A. A., Saffman, P. G. & Rogallo, R. S. 1993 The structure of intense vorticity in isotropic turbulence. *J. Fluid Mech.* **255**, 65–90.

MANDELBROT, B. B. 1974 Intermittent turbulence in self-similar cascades: divergence of high moments and dimension of the carrier. *J. Fluid Mech.* **62**, 331–358.

MANDELBROT, B. B. 1990 Negative fractal dimensions and multifractals. *Physica* A **163**, 306–315.

MANDELBROT, B. B. 1991 Random multifractals: negative dimensions and the resulting limitations of the thermodynamic formalism. *Proc. R. Soc. Lond.* A **434**, 79–88.

MENEVEAU, C. 1991 Analysis of turbulence in the orthonormal wavelet representation. *J. Fluid Mech.* **232**, 469–520.

MENEVEAU, C. & SREENIVASAN, K. R. 1987 Simple multifractal cascade model for fully developed turbulence. *Phys. Rev. Lett.* **59**, 1424–1427.

MENEVEAU, C. & SREENIVASAN, K. R. 1991 The multifractal nature of turbulent energy dissipation. *J. Fluid Mech.* **224**, 429–484.

OTT, E. & ANTONSEN, T. M. 1989 Fractal measures of passively convected vector fields and scalar gradients in chaotic fluid flows. *Phys. Rev.* A **39**, 3660–3671.

OTT, E., GREBOGI, C. & YORKE, J. A. 1989 Theory of first order phase transitions for chaotic attractors of nonlinear dynamical systems. *Phys. Lett.* A **135**, 343–348.

PEITGEN, H., JURGEN, H. & SAUPE, D. 1992 *Chaos and Fractals: New Frontiers of Science*. Springer.

PRASAD, R. R., MENEVEAU, C. & SREENIVASAN, K. R. 1988 The multifractal nature of the dissipation field of passive scalars in fully turbulent flows. *Phys. Rev. Lett.* **61**, 74–77.

PRASAD, R. R. & SREENIVASAN, K. R. 1990 Quantitative three-dimensional imaging and the structure of passive scalar fields in fully turbulent flows. *J. Fluid Mech.* **216**, 1–34.

SHIVAMOGGI, B. K. 1992 Multi-fractal aspects of the intermittency corrections to the spectrum of temperature fluctuations in isotropic turbulence. *Phys. Lett.* A **168**, 47–54.

SOUTHERLAND, K. B. & DAHM, W. J. A. 1994 A four-dimensional experimental study of conserved scalar mixing in turbulent flows. *Report No. 026779-12*, Department of Aerospace Engineering, The University of Michigan, Ann Arbor, MI.

SOUTHERLAND, K. B. & DAHM, W. J. A. 1996 Fully resolved four-dimensional measurements of the small-scale structure of passive scalar mixing in turbulent flows. Submitted to *J. Fluid Mech.*

SOUTHERLAND, K. B., DAHM, W. J. A. & DOWLING, D. R. 1995 Experimental results for the high wavenumber spectral structure of scalar mixing in turbulent shear flows. In *Proc. 10th Symp. Turb. Shear Flows*, Pennsylvania State University, University Park, PA.

SREENIVASAN, K. R. 1991*a* Fractals and multifractals in fluid turbulence. *Ann. Rev. Fluid Mech.* **23**, 539–600.

SREENIVASAN, K. R. 1991*b* On local isotropy of passive scalars in turbulent shear flows. *Proc. R. Soc. Lond.* A **434**, 165–182.

SREENIVASAN, K. R. & PRASAD, R. R. 1989 New results on the fractal and multifractal structure of the large Schmidt number passive scalars in fully turbulent flows. *Physica* D **38**, 322–329.

SREENIVASAN, K. R. & STOLOVITZKY, G. 1995 Turbulent cascades. *J. Stat. Phys.* **78**, 311–333.

SU, L. K. & DAHM, W. J. A. 1996*a* Scalar imaging velocimetry measurements of the velocity gradient tensor field in turbulent flows. Part I: Assessment of errors. *Phys. Fluids* **8**, 1869–1882.

SU, L. K. & DAHM, W. J. A. 1996*b* Scalar imaging velocimetry measurements of the velocity gradient tensor field in turbulent flows. Part II: Experimental results. *Phys. Fluids* **8**, 1883–1906.

TSINOBER, A., KIT, E. & DRACOS, T. 1992 Experimental investigation of the field of velocity gradients in turbulent flows. *J. Fluid Mech.* **242**, 169–192.

VARÓSI, F., ANTONSEN, T. M. & OTT, E. 1991 The spectrum of fractal dimensions of passively convected scalar gradients in chaotic fluid flows. *Phys. Fluids* A **3**, 1017–1028.